The Impact of Spatial Variation of Westerlies On Comprehensive And Extreme Precipitation Over Iran

Nabi Mirzaei

std_nabi_mirzaei@khu.ac.ir

University of Kharazmi Tehran https://orcid.org/0000-0001-8209-5653

Bohloul Alijani

Kharazmi University

Zahra Hejazizadeh

Kharazmi University

Mohammad Darand

University of Kurdistan

Mohammad Hossein Naserzadeh

Kharazmi University

Research Article

Keywords: sinuosity, westerlies, variation, extreme precipitation, Iran.

Posted Date: November 12th, 2021

DOI: https://doi.org/10.21203/rs.3.rs-976324/v1

Abstract

This study analyzed the impact of spatial variation in westerlies on widespread and heavy precipitation over Iran using the sinuosity index. Four groups of datasets were used for the period from 1979 to 2020, containing the gridded geopotential height, specific humidity, precipitation data, and the Arctic Oscillation (AO) and North Atlantic Oscillation (NAO) teleconnection patterns. The results demonstrate that the trend in sinuosity variation has been decreased during the 1979-1999 sub period but increased from 2000 to 2020. The analysis of the trend in cumulative sinuosity for the above two sub periods indicates that sinuosity rate has been greater in the latter than in the former all over the year except in October. The overall trend in sinuosity variation exhibits an increase by 0.0018, significantly. Maximum sinuosity can be observed in January, March, and December, and minimum sinuosity is seen in October. The relationship between heavy precipitation and sinuosity suggests that daily precipitation has increased by 3 mm with a rise of 0.2 in the value of sinuosity, monthly precipitation by 10 mm, and the annual value by 38 mm. Thus, the rate of correlation between sinuosity and precipitation over Iran equals to 0.74. Sinuosity increase in the 0-70° E range indicates an increase in wave depth and the occurrence of a cut off low. The most important factor in the persistence of widespread extreme precipitation has been the formation of these lows in the 20-40°E and 20-35°N ranges.

1 Introduction

There is evidence that the occurrence of weather extremes including heavy, flood-like precipitation has led to large amounts of mortality and financial harm in recent years (Davenport 2021; Huang et al. 2021). Climate change can increase the frequency and severity of extreme events including heavy precipitation (Swain et al. 2020; Sen Roy 2009). It is therefore essential to conduct scientific research in that regard (Tabari 2021; Davenport et al. 2021; Singh 2013; Allen 2002). Moreover, global average air temperature has an increasing trend, which is more intense in the North Pole than in the Northern Hemisphere (Hamidianpour and khosravi 2020). This causes changes in the North Pole surface ice. The fast Arctic warming will weaken the polar vortex, shifting cold weather down to lower latitudes, and can enhance the Arctic and increase atmospheric turbulence and the occurrence of weather extremes under the influence of a positive feedback (Barnes 2013; Liu et al. 2012). Atmospheric interactions and their impact on precipitation frequency and intensity (Lauterbach et al. 2014; Bogardi et al. 1994). Can be identified through identification of the variation in large-scale patterns (Vicente-Serrano and Moreno 2006:1429). One of the most important effects of global warming is the variation in tropospheric circulation in the middle layers of the atmosphere and its dynamic patterns (Abatzoglou et al. 2016; Cattiaux 2016). Given Iran's location in the subtropical Azores High region in the South and on the westerly direction in the North, it is influenced alternatively by the northern margin of the former system and the southern margin of the latter flow. Factors associated with precipitation variability over Iran include the behavior of dynamic patterns under the influence of large-scale atmospheric circulation. The dominant pattern and major stimulus upon occurrence of precipitation in Iran includes the westerlies and resulting precipitation cyclones. Dynamic cyclones and anticyclones emerge at the land surface as a result of the dominance of

westerly flow in the middle layers of the atmosphere. During the high subtropical retrogression in fall to latitudes further to the south, the extension of vorticity increases from the North to the South. The beginning of fall is regarded as the initiation of westerly activity in Iran, and positive vorticity extends further over the country as these winds dominate, providing the requirements for occurrence of precipitation (Darand and Mirzaei 2018). Precipitation in Iran is characterized by qualities such as being seasonal, short-term, particular to the cold season of the year, and showery within a short period (BabaieFini and Farajzadeh 2002). In the past decade the behavior of weather systems over Iran has undergone plenty of variation in terms of rate and intensity, and precipitation has occurred as widespread and heavy showers (Alijani et al. 2019). Severe variability is one of the most important features of precipitation in Iran, to the extent that a region may experience quite different conditions in two years. It is actually the factors effective on atmospheric circulation interaction that cause weather diversity, and those factors need to be examined for investigation of the diversity (Boucher 1976). The analyses of atmospheric patterns upon the occurrence of widespread, extreme precipitation in Iran in recent years indicate intense meridian variation in westerlies (Bifurcation) and persistent blocking. In these conditions, the atmospheric patterns are laid out so that westerlies are split into two branches, and the phenomenon of blocking occurs (Alijani et al. 2019). Westerlies are known as highly important representations of general atmospheric circulation that take shape as a result of large-scale pressure variation in the atmosphere and ocean. The dominance of the westerly jet in the cold season of the year plays an inevitable role in middle-latitude regions in wet and dry periods (Hitchman and Rowe 2021). Examination of the impacts of westerly frequency and wave intensity well justifies the variability in weather systems, wet and dry periods, precipitation and temperature extremes, and atmospheric humidity. The spatial variation in westerly flows is effective on the increase in air vorticity and the formation of precipitation-inducing systems and their locations. Previous research performed in that regard has emphasized the role of the blocking pattern in enhancement of the meridian component of the westerly flow, including Zolfaghari et al. (2012); Azizi et al. (2018); Hombari (2020). Studies have also been conducted outside Iran by Lupo (2008); Miyakoda et al. (1983), Using statistical indices and methods. However, none of the domestic investigations has addressed the role of spatial variation in westerlies on the variability in the atmospheric waves effective on precipitation over Iran. It has only been the relationship between the blocking pattern frequency and precipitation that has been studied, where westerlies take shape as a result of pressure oscillation in Atlantic Ocean, and play an important role in the development and extension of precipitation systems in Iran by moving from the West to the East. The frequency of storms and the variation in atmospheric waves under the influence of the variation in the Atlantic atmospheric patterns greatly contribute to the changes in climatic elements in mid-latitudes and human activity (Bers and Conrad 1994). Moreover the studies conducted by Schinke (1993); Stein and Hens (1994); Bacon and Carter (1991) indicate the relationship between large-scale climatic patterns and the increase in mid-latitude cyclones (Martin et al. 2016). It is of great significance in the prediction of extreme precipitation to analyze the impacts of variation in westerlies in the investigation of the mechanism governing the occurrence of precipitation (Ding 2019) and heavy precipitation under the formation of blocking (Krishnamurti et al. 2002; Faris and Moody 1999). Furthermore, the spatial variation in westerlies in the increasing/decreasing movement of waves toward the Mediterranean intensifies the air mass vorticity,

cyclogenesis, and increase in cyclone energy (Tyrlis et al. 2015). Given the significance of the spatial variation induced by westerlies in atmospheric elements such as precipitation, it is far more important to study westerlies upon the occurrence of climate change. The variation in westerlies, which is represented as increase in wave depth and amplitude, leads to a rise in the phenomenon of blocking and consequent persistence in precipitation (Castillo 2020). The variable nature of atmospheric waves in large scale causes great variation in weather system circulation and precipitation disorder (Cattiaux et al. 2016). Investigation of atmospheric wave oscillation in the upper layers of the atmosphere is quite versatile in the assessment of weather change quality (Van Loon and Williams 1976) and understanding of the variations in land surface elements including weather extremes over Iran. The present research investigated the sinuosity index of westerlies at 500 hPa in the widespread precipitation over Iran. Cattiaux et al. (2016) were among the first researchers who studied sinuosity values in the upper layers in mid-latitudes. The results indicated a close relationship between daily sinuosity and AO in the cold season of the year. Martin et al. (2016) also conducted a more comprehensive study of tropospheric waves with the sinuosity index for different latitudes and the relationship between AO and sinuosity. The results demonstrated that there was no significant relationship between the sinuosity index and the Arctic oscillation. Martin has introduced the sinuosity index as an important index for identification of tropospheric westerly waves. Vavrus et al. (2017) have also utilized the sinuosity method for specification of weather extremes over the United States. Along the same lines, Hojati and Masoodian (2021) investigated the relationship between sinuosity and minimum temperature over Iran, indicating an increase in westerly sinuosity values. No research has been focused so far on the impact of westerly waves on precipitation over Iran. The role of westerlies in precipitation over Iran has been investigated with other approaches such as examination of the spatial variation in westerlies or in Mediterranean troughs (Alijani and Nezamati 2014). Many aspects of the impact of westerlies on the atmospheric synoptic pattern effective on mid-latitude precipitation including that over Iran seem to have remained unknown. Moreover, sinuosity variability in the period of AO/NAO can provide an appropriate approach to prediction and understanding of the relationship between atmospheric circulation effective on precipitation and teleconnection oscillation. AO/NAO is of great significance in examination of the variation in seasonal precipitation (Dorn 2003) and the findings of Pavlovic (2012) and Hu (2020) indicate the relationship between precipitation and AO/NAO in the Northern Hemisphere. Since no study has been conducted so far on the sinuosity-precipitation relationship over Iran, the present research investigated the relationship between the frequency and intensity of sinuosity at 500 hPa and the widespread and heavy precipitation over the country. It also examined the relationship between the two teleconnection patterns of AO/NAO and 500 hPa sinuosity.

2 Data And Method

For analysis of the impact of westerly sinuosity on widespread precipitation over Iran, three classes of data were used, including (synoptic and rain gauge) station data, data from the upper layers of the atmosphere, and AO and NAO data. The station precipitation data involved daily data from 250 synoptic and rain gauge stations (Fig. 1). The data were sorted for identification of days with widespread

precipitation, defined as days when precipitation occurs at 50% of the stations. Heavy precipitation was identified in terms of the 95th percentile threshold. The network data involved the variables of geopotential height and specific humidity with a spatial resolution of 0.25 × 0.25 degrees of arc extracted from the ECMWF-ERA5 dataset. A large number of studies have been conducted recently to investigate the roles of atmospheric variables on climatic conditions based on the latest version of the above dataset, including Dullaart et al. (2020); Delhasse et al. (2020); Di Napoli (2021) etc. The data on the teleconnection patterns of AO and NAO were received from the NOAA Climate Prediction Center. Figure 1 shows the map of long-term mean precipitation over Iran during the 1979-2020 period.

For examination of the variation in sinuosity values, the period under investigation was divided into two equal sub periods, including 1979-2000 and 2001-2020. The sinuosity values for each sub period were calculated, followed by the mean rate of sinuosity in each (Fig. 3). The data on geopotential height at 500 hPa were used for identification of the variation in westerlies. The middle level of the atmosphere, 500 hPa correspond to the greatest atmospheric mass, at which westerlies assume the highest velocity, and are closest to the trough level. Therefore, it is of greater significance in investigation of westerlies (Alijani et al. 2019; Barnes and Polvani 2013). In the present study, the sinuosity method was used for measurement of the sinuosity of middle tropospheric flows. Given that westerly flows assume sinuosity within the Atlantic range, the 10°N-60°N 80°W-70°E kernel range was considered at first for calculation of mid-layer sinuosity. Then, the sinuosity values were obtained for the 10°N-60°N 0°E-70°E range upon widespread and heavy precipitation over the country. Introduced by Cattiaux et al. (2016) and Martin et al. (2016), the method of sinuosity was first used by Hojati and Masoodian (2021) for investigation of atmospheric waves in the tropospheric layer and the impacts of the fast Arctic warming and variation in atmospheric circulation on temperature variation in Iran. Sinuosity is defined as the ratio of the curve length of a height contour in the middle layers of the atmosphere to the perimeter of the corresponding latitude. It is similar to the versatile method of sinuosity in geomorphology, where the height contour is nearly of the same length as a spiral river path, and the corresponding latitude is nearly of the same length as the shortest distance of the same point on the river path (Cattiaux et al. 2016; Martin et al. 2016; Hojati and Masoodian 2021). For calculation of cumulative sinuosity, the most frequent height contour curves upon widespread precipitation over Iran were first selected. The frequency of 500hPa curves within the borders of Iran upon widespread and heavy precipitation was selected (Fig. 2). For avoidance of repetition of the selected contours, only those of 558, 565, and 575 dam were adopted in the process of drawing the contour map. The 500hPa contour can be obtained in the calculation of sinuosity along the latitude that leads to variation in atmospheric flows. Thus, the greater the variation toward latitudes, the severer the blocking, cut off low, and cut off high. The cut off lows and high can be identified on the high-contour maps using the sinuosity index. Therefore, the frequency of cut off lows during the period of study was also examined. The trend in daily, monthly, and annual variation in sinuosity in the period of study was investigated using the Mann-Kendall test, along with the variation in sinuosity in different phases of AO and NAO. Finally, the relationships between different values of the sinuosity index and precipitation over Iran were obtained for the winter and fall months using Pearson's correlation coefficient at the confidence level of 95%.

After the curves and the ranges relevant to each were selected, the equivalent latitude was calculated, which is the latitude bounding an area equal to that to the north of the relevant height contour curve, obtained by the following equation

$\varnothing_E$ =$\arcsin[1 - \frac{A}{2{=}\pi Re^2}]$ (Martin et al. 2016)

In this equation, A is the area bounded by the height contour curve, and R2 is the Earth radius. Then, the following equation was used for calculation of cumulative sinuosity.

$Asin = \frac{L_{iso1}+L_{iso2}+L_{iso3}+L_{iso4}}{EL_{\varphi 1}+EL_{\varphi 2}+EL_{\varphi 3}+EL_{\varphi 4}}$(Martin et al. 2016)

In this equation, L is the length of the relevant height contour curve, and EL is the length of the equivalent latitude. The length is the shortest possible distance between the beginning and end points of the orbit. The length of a specific height contour curve is obtained using the following equation as the sum of the segments over each 0.25×0.25 grid box.

$$=\operatorname{acos}\left[sin_{\boldsymbol{\phi 1}} sin_{\boldsymbol{\phi 2}} + cos_{\boldsymbol{\phi 1}}\, cos_{\boldsymbol{\phi 2}} \cos\left(\gamma_{\mathbf{2}} - \gamma_{\mathbf{1}}\right) R_{\mathbf{e}}\right] l$$

In this equation, (φ1, (1)_γ) and (φ2, (2)_γ) are the coordinates of the points at which the height contour curve has intersected the boundaries of the network of longitudes and latitudes, and Re is the Earth radius. According to these definitions, the minimum value of sinuosity is about 1, which indicates an orbital flow, and any increase in this value denotes a rise in the sinuosity value of the flow (Hojati and Masoodian, 2021). In the calculation of sinuosity at a contour of 565 dam, for example, the enclosed area is turned into that of a circle, and the wavelength ratio of the 565 dam curve is turned into the circle perimeter.

3 Results

Figure 3 shows long-term mean sinuosity for winter and fall during the 1979-2020 period. As can be observed, the value of sinuosity is maximized in winter over mid-latitudes, particularly over Iran. Thus, the conditions required for atmospheric turbulence and precipitation are met, and long-term mean sinuosity index for winter amounts to 1.35. Among the winter months, maximum sinuosity is observed in January and March (Fig. 4). As the subtropical high shifts back toward lower latitudes in fall, westerly flows tend to extend in the same direction and enforce the conditions required for meridian wind. The consequent formation of troughs in the middle layers of the atmosphere amplifies instability, and the mean rate of sinuosity amounts to 1.31 in fall. Among the fall months, maximum sinuosity is observed in December and November (Fig. 4). In this season, the location of the subtropical high and its orbital and meridional extension are of great significance in specification of sinuosity in the middle layers of the atmosphere. Thus, the value of sinuosity in the atmosphere increases in October as the high shifts southward to lower latitudes.

Mean monthly sinuosity for the winter and fall months in the 1979-1999 and 2000-2020 periods indicate the variation in sinuosity during these two sub periods. Similarly in annual scale, the value of sinuosity exhibits great variation within an interval of two years. These changes are made as a result of the nature of large-scale atmospheric patterns; thus, the variation is effective in the temporal and spatial distribution of climatic factors such as precipitation. The figure for mean sinuosity in January indicates that the parameter has decreased at the end of the first sub period with respect to the initial years, and has increased at the end of the second sub period. The variation in February is similar to that in January. The highest value of sinuosity in the first sub period has occurred in 1987, and that in the second sub period is observed as 1.46 in 2019. In March, there have been higher values of sinuosity in the second sub period than in the first in most of the years. Since 2012, mean sinuosity has increased in this month. Unlike for the other months, the rate of sinuosity in the 2000-2020 period exhibits a decrease for October with respect to that in 1979-1999. The highest value of sinuosity in this month is observed between 1979 and 1988. For November, sinuosity exhibits a decrease in the 1990s with respect to the mean value for the entire period, while an increase is observed for the 2010s. In December, the maximum value of sinuosity in the first sub period has occurred in 1987, while sinuosity rate has been higher in 2004, 2019, and 2018 than in the other years in the second sub period. Mean sinuosity is greater for December than for November and October. The values of mean monthly cumulative sinuosity indicate that higher rates of sinuosity are observed for January, March, and December than for the other months under examination. Mean sinuosity rate has been greater in the second sub period than in the first. Throughout the period of 42 years, sinuosity has been maximal in 2019 and minimal in 2010 (Fig. 4).

The values of mean monthly sinuosity for the period under investigation Figure 4 indicate that maximum sinuosity is observed for January, March, and December, while the minimum has occurred in October. Moreover, increase is observed in sinuosity for all the 500hPa contours, simultaneous with the increase in monthly sinuosity. Cases of increase in sinuosity by more than 1.3 exhibit increase in all the contours and decrease in their differences, while greater differences are observed in the rate of sinuosity for months with lower values of mean sinuosity (Fig. 5). In January, March, and December, where 500hPa sinuosity exhibits increase, the same trend is observed for all the contours. For October, with lower values of sinuosity, the highest values are observed in the 575 and 565 dam contours and the lowest in the 558dam contour, since westerly flows are weakened in October with respect to those in the other months. For this month, it is of great significance in specification of mid-layer sinuosity and atmospheric instability when the flows extend southward. Overall, mean sinuosity is greater in the 575 dam contour than in the 565 and 558 dam contours.

The values of mean monthly sinuosity in the 2000-2020 and 1979-1999 periods, in Table 1, indicate increasing significant trends in sinuosity in all the months except for October at 95% confidence level, with the greatest increase observed in January and March, by 0.002 and 0.003, respectively. Mean sinuosity during the second sub period, with a rate of 1.29 is greater than that in the first, with a rate of 1.28 representing an average growth rate of 0.014.

Table 1
The difference between the sinuosity values of the first period (1999 to 1979) and the second period (2000 to2000)

month	First Period (1979-1999)	Second Period (2000-2020)	Second Period- first Period
JAN	1.31	1.33	0.02
FEB	1.29	1.30	0.01
MAR	1.30	1.33	0.03
OCT	1.19	1.2	-0.01
NOV	1.29	1.29	0.01
DEC	1.31	1.33	0.02

Figure 6 shows mean seasonal 500hPa sinuosi. Clearly, mean seasonal sinuosity has reached to more than 1.3 in 1993 and 1997 but dropped to less than 1.3 in 1999 and 1981, where it exhibits the lowest values in the first sub period. By contrast, there is a considerable initial decrease in sinuosity in the second sub period, which has amounted to the highest values throughout the 42-year period in the final years, particularly in 2011, 2015, and 2019. Such an increase in sinuosity indicates intensified meridian 500hPa westerly flows, while a decrease in sinuosity raises the orbital flow and stability. An increase in sinuosity causes the flows to tend to extend toward lower latitudes, which can increase the probability of occurrence of the blocking phenomenon (Hojati and Masoodian 2021). Mean seasonal sinuosity during winter indicates an increasing trend in sinuosity. The parameter has assumed the lowest values throughout the period in 1989 and 2010 and the highest in 1993, 2011, 2015, and 2019. Thus, the values of mean seasonal sinuosity suggest that sinuosity has been greater in winter than in fall, although the monthly rate in December equals those observed for the winter months (Table 1).

The dynamic patterns effective on precipitation can vary greatly under the influence of NO oscillation (Dorn 2003). The relationships between AO and NAO and precipitation (Bannayan 2010; Yadav 2009; Gong et al. 2014) and anomaly in sinuosity and the above indices, shown in Fig. 7, indicate close correlations between sinuosity and AO and NAO in both sub periods, where positive anomaly in AO and NAO has relatively increased sinuosity (Fig. 7a). As the above indices have turned negative in 2010, sinuosity has decreased to a minimum. With an increase in sinuosity by 0.2, daily precipitation has increased by 3 mm, monthly precipitation by 10 mm, and annual precipitation by 38 mm. There has been a closer relationship between sinuosity and teleconnection indices in the second than in the first sub period. Overall, the relationship between sinuosity and the AO index has amounted to 0.65 and that for NAO to 0.52. Moreover, the statistical relationship between sinuosity in the middle layers of the atmosphere and annual precipitation has exceeded 0.74, indicating a close relationship between sinuosity and precipitation in the study area (Fig. 7b). The increase in the sinuosity index values of 500 hPa flows over Iran has been accompanied by positive anomaly in precipitation. It can be stated in general that precipitation over Iran increases/decreases as AO and NAO assume positive/negative

phases, and sinuosity rises in the middle layers of the atmosphere, indicating that AO and NAO are effective in the atmospheric pattern variation in the middle layers (Fig. 7a).

3.1 The relationship between sinusoidal and extreme precipitation

As mentioned in the section on the data and methodology, the sinuosity values were calculated for two kernel ranges, including a large one, i.e. 10°S to 60°N 80°W to 70°E, and a small one, i.e. 10°S to 60°N 0 to70°E. Figure 8 shows mean daily sinuosity upon widespread and heavy precipitation over the country for the small range. In these conditions, sinuosity has been greater in all the months under examination in the 575 and 565dam contours than in the others. In other words, sinuosity exhibits the highest frequency over Iran in these contours. In an examination of the 575, 565, and 558dam contours, the greatest variation is observed in the 558dam contour. In October and November, the above contour accounts for the lowest sinuosity, while the 575dam contour exhibits the highest. In March and January, the same sinuosity is observed for the 558 and 575dam contours, and atmospheric sinuosity could be identified in these months in all the 500hPa contours due to the high intensity of atmospheric waves (Fig. 3). During the second sub period, sinuosity has been less in the 558dam contour than in the first sub period but greater in the other contours. The decrease in sinuosity in this contour may be accounted for by the enhanced high pattern in fall, functioning as a barrier against precipitation flows and systems, which would be consistent with the decreasing trend in sinuosity observed in this research for October (Table.1). However, the above claim requires further investigation. Overall, mean cumulative sinuosity during the study period has been 1.48 in the 575dam contour, 1.40 in the 565dam contour, and 1.30 in the 558dam contour. Over the entire period of investigation, the above contours exhibit increase in 500hPa sinuosity in the 2010s, maximized in 2019 (Fig. 8).

Figure 9 shows anomaly in the frequency of rainy days and sinuosity. The results of examination of sinuosity upon widespread precipitation indicate that the frequency of rainy days has varied consistently with the variation in sinuosity. For a change of 0.2 in sinuosity, the frequency of rainy days has changed to three days more/less than the mean value. Similarly in Figure 8, positive anomaly is shown to have occurred in the frequency of rainy days as sinuosity has increased in 1990, 1984, 2010, 2013, and 2019.

Mean daily sinuosity upon widespread and heavy precipitation over the country indicates annual and monthly variation. As 500hPa westerly flow sinuosity has increased/decreased, the frequency of days with heavy precipitation has increased/decreased. Mean sinuosity has been 1.55 during the 1979-1999 period and 1.59 in the following period of 21 years, i.e. 0.4 more in the second sub period than in the first (Fig. 10a).On the other hand, the frequency of widespread and heavy precipitation over the country has amounted from 6.95 in the former to 7.22 in the latter, indicating an increase by 0.277. In general, the increase in 500hPa sinuosity rate justifies the rise in heavy precipitation (Fig. 10b).

3.2 Case studies

For explanation of the variation in sinuosity in the middle layers of the atmosphere, four of the patterns leading to widespread and heavy precipitation over Iran were selected, for which the sinuosity index was calculated. Then, the 500hPa geopotential height pattern and 850hPa specific humidity were drawn. Widespread precipitation has occurred in most regions as heavy precipitation, as it has persisted with high intensity for several days. An examination of the geopotential height map indicates that westerlies have been split to two branches, northward and eastward, upon widespread precipitation following a formation of atmospheric blocking, when the 500hPa cut off low has caused the flows to shift eastward at a low rate, increasing the sinuosity index and precipitation in the study area. Mid-layer cut off lows have taken shape in all the examined patterns, increasing sinuosity due to the meridian extension of flows toward lower latitudes. An examination of sinuosity maps upon heavy precipitation indicates the formation of two blocking patterns with separate cores to the east and west of the Mediterranean. A similar examination for widespread precipitation demonstrates that it has occurred in more than 80% of cases under the influence of the bipolar pattern. Specifically, the Specifically, the initial blocking core has taken shape over Eastern Atlantic and Western Mediterranean following an amplification of the meridian index of high flows, and the second cutoff low core has taken shape over the Mediterranean within the next 24 hours, leading to widespread precipitation over Eastern Mediterranean, including Iran, following an amplification of vorticity and injection of moisture from humid regions. The initial core has extended westerlies toward lower latitudes, and increased high atmospheric wave amplitude, enabling atmospheric instability by amplifying flows and raising wind speed. Table 2 shows the times when widespread and heavy precipitation begins and ends and the atmospheric patterns causing them.

Table 2

Start/End Dates selected Case for inclusive comprehensive and heavy rainfall and Average rainfall of stations during the period, atmospheric pattern causer to precipitation and their spatial position (the first position is the North Atlantic blocking and the second position is the eastern Mediterranean blocking)

Start Time	End Time	Average precipitation(mm)	Atmospheric patterns	blocking core 1 location	blocking core 2 location
1Feb 1993	6 Meb1993	36	Blocking, Eastern Mediterranean Sea through, cut of low	20N 35 N -15W 0	20N 35N 30E 50E
24Mar2003	30Mar2003	29	Blocking, westerly bifurcation, Cut of low	20N 35N -30W 15E	15N 35N 15E 45E
23Dec2004	30Dec2004	30.03 m	Blocking(cut of low)	20N 40N -15W 15E	20N 35N 30E 50E
19Mar2019	31Mar2019	42.1 m	Blocking(Cut of low), westerly bifurcation	30N 45N -30W 0	25N 40N 10E 48E

3.3 Case 1

Patterns adopted upon widespread precipitation over Iran, which have led to extreme or ultraheavy precipitation in some cases. In the first instance, concerning February 1993, a powerful cutoff low pattern has been established over Eastern Mediterranean, and an initial low core has taken shape at the same time over Eastern Mediterranean, at 30°N. These conditions have caused the extension of flows toward lower latitudes, trough deepening, and an increase in upward flow shift. The cores of the two deep troughs separated through northward stack extension at 15°E can be observed within 15N 40°N. The mid-layer inverse *S* blocking pattern causes cold weather to pour down from higher latitudes toward the Mediterranean, and then brings about widespread precipitation over Iran as the pattern cycles to inject moisture from the Mediterranean and Atlantic. A value of 1.48 is observed for the sinuosity index upon precipitation, and western flows have extended to 20°N following trough deepening (Fig. 11a).These series of conditions have induced 36 mm of precipitation at an average station. The above pattern has caused greater precipitation to occur in this period in the West, Southwest, Northeast, and western part of Caspian Sea than in other regions. The spatial distribution of precipitation in this period well demonstrates that it has spread widely over most parts of the country (Fig. 11c).

3.4 Case 2

Like the above instances, the sinuosity pattern for March 2003 has caused heavy precipitation over Iran, leading to prolonged persistent precipitation during a seven-day period of blocking. Some of the stations have recorded 100 mm of precipitation within this period, when the largest amounts of precipitation have concerned regions located along Zagros Mountains, in the Northwest, and along the Caspian coasts, in that order, indicating unstable conditions over different regions from the Southwest to the North. Sinuosity has amounted in this period to 1.48, bringing about unstable conditions as precipitation in Eastern Mediterranean under the influence of westerlies extended to 15-20°N. Over the Mediterranean, blocking has caused the flows to be split into two branches, northern and southern. The latter has extended southward to lower latitudes as a result of blocking in Fig. 12a. The sinuous flow pattern from the West to the East, involving sinuosity over Eastern Atlantic and Western and Eastern Mediterranean, indicates an increase in wave power and in upward shift in the upper layers of the atmosphere. Upon widespread precipitation over the country, the greatest humidity can be observed over the western half. The mid-layer trough is located in average at 35°N upon precipitation in the region. The spatial location of this trough over Eastern Mediterranean and Northern Red Sea, well justifies the increase in humidity for heavy precipitation (Fig. 12c).

3.5 Case 3

The 500hPa geopotential height pattern indicates the high meridian extension at 30°E up to 40°N, which has intensified pressure gradient over the eastern half of Northern Atlantic, indicating great divergence in temperature, pressure, and wind speed. The decrease in meridian flows in Western Mediterranean has led to a tilted trough axis and an increase in wavelength. Stack extension from Southeastern to Northeastern

Mediterranean has amplified the Eastern Atlantic trough, evolved with the increase in mid-layer trough flows in Eastern Mediterranean(Fig. 12a). The rise in the amplitude and depth of 500hPa flows can well be observed in the geopotential height pattern, causing an increase in the occurrence of blocking. There have also been particular conditions in terms of precipitation over Iran in December 2004 due to the formation of the bipolar mid-layer cut off low pattern in Eastern and Western Mediterranean with a sinuosity value of 1.49, when an extensive part of the country has received precipitation. In certain regions, total precipitation has amounted to more than 100 mm upon formation of this pattern. Moreover, the values of specific humidity upon precipitation indicate moisture flux from the Southern waters, particularly Indian Ocean and Oman Sea, with the requirements for heavy precipitation met despite the intense conditions for upward shift in the middle layers of the atmosphere. Maximum humidity is observed in the western half of Iran as 8 g/kg (Fig. 12b).

3.6. Case 4

As mentioned in the examination of the previous pattern, widespread and ultraheavy precipitation has occurred over the country in March 2019, when the persistence of instability and increase in atmospheric sinuosity with multiple days of duration have caused ultraheavy precipitation to occur in the western and northeastern parts of Iran as sinuosity has been amplified, and cut off lows have taken shape in the middle layers of the atmosphere. At certain stations, the recorded precipitation has amounted to more than 300 mm in Fig. 6c, which equals half of the annual precipitation for some of the stations (Alijani et al. 2019). A daily sinuosity rate of 1.6 can be observed for this period, which is regarded as a wet one with high precipitation. Instability has been experienced in this period in a large number of regions in Iraq, Saudi Arabia, and Turkey as well as in Iran. An examination of the geopotential height pattern indicates the formation of a highly powerful cut off low over the Mediterranean, where the increase in the prevalence of flows and trough deepening have intensified instability over the country. The geopotential height pattern demonstrates that two troughs have taken shape over Eastern and Western Mediterranean, which have become distinguishable following a stack extension in Western Mediterranean. The trough in the East has split westerly Bifurcation, due to the 500hPa blocking. The southern branch of westerlies, in Eastern Mediterranean, has induced cut off lows, the appropriate location of which along with their stretch over Red Sea and the humidity of the Mediterranean has brought about moisture flux from Red Sea. This scarce pattern has caused the highest precipitation to occur over the western parts of Iran. The flows correlated as a result of the developed pattern have amplified humidity upon heavy precipitation in the lower layers of the atmosphere, and plenty of moisture has arrived in the region from the Mediterranean, Red Sea, Persian Gulf, and Oman Sea upon persistence of precipitation. Maximum humidity is observed as more than 8 g/kg as the pattern induces precipitation over the western half of Iran, which occurs in larger amounts than that induced by other patterns. The location of cut off lows and the persistence and high intensity of precipitation in March 2019 has caused widespread and heavy precipitation to occur over the country (Fig. 14c).

3.7 Blocking

As stated earlier, the blocking pattern and the low middle layers of the atmosphere have played a major role in the occurrence of widespread and heavy precipitation over Iran. Fig. 15a shows the best case of widespread and extreme precipitation occurring over the country following the formation of mid-layer cut off lows. Under these conditions, cutoff lows have caused deep troughs to take shape in the middle layers of the atmosphere, the outermost contour of which has been located at 15°N. The lows have covered a spatial range around 15°N 10°E. For the study period, the occurrence of widespread and heavy precipitation has been consistent with the location of cut off lows within 20°N-35°N, 20°E-40°E, which has led to extreme precipitation over Iran in most cases. This demonstrates that the location of cut off lows plays an important role in the persistence and intensified occurrence of heavy precipitation over the country.

An analysis of their frequency of occurrence within the 500hPa 10°N-60°N 0 -70°E kernel indicates that they have occurred with an increasing trend throughout the study period. Increase in the frequency of cut off lows is highly consistent with 500hPa sinuosity. One of the most important factors that can control the frequency, intensity, and duration of cut off low activity is westerly flow, the variation and gradient in which leads to the separation of cut off lows. A low-pressure closed cyclonic eddy separated from the main jet stream (Singleton et al. 2007), a cut off low functions as a system that interrupts westerly flow upon occurrence of wet and dry periods (Muñoz and Schultz 2021). During the study period, cut off lows have occurred more frequently as 500hPa sinuosity has increased, and far more frequently in the 2000-2020 period than in 1979-1999, particularly in 2000-2003, 2015, and 2019. This highlights the role of sinuosity in the occurrence of atmospheric blocking. Furthermore, the frequency of blocking could have a significant impact on the intensity of heavy precipitation in Iran due to its arid and semi-arid climate and the showery nature of precipitation therein (BabaieFini and Farajzadeh 2002). Given the importance of blocking in the occurrence of precipitation over Iran, it is essential to conduct further studies on the role of climate change in the variation in atmospheric patterns effective on the occurrence of blocking.

The relationship between Extreme and Comprehensive precipitation and sinuosity in Iran

Figure 17 shows the relationship between monthly sinuosity rate and precipitation during the study period using Pearson’s correlation coefficient at the confidence level of 95%. As can be observed, there has been a positive relationship between widespread precipitation and sinuosity over a large part of Iran. In other words, precipitation has assumed an increasing trend there as atmospheric sinuosity has risen. The relationship has been far closer in all the months in the western and northern halves and the Southwest than in the other regions. Moreover, the rate of correlation between precipitation and 500hPa sinuosity has been higher over the western half of the country in March and November than in the other months. More regions have received precipitation in February along with increase in sinuosity, and there has been poorer relationship between widespread precipitation and sinuosity in the southern and southeastern regions. In all the months under examination, there has been maximal relationship between sinuosity and widespread precipitation in the western half and northern parts of Iran. It can be stated in general that the variation in sinuosity provides an appropriate index for investigation of the impact of variation in westerly

flows on the occurrence of precipitation over the country, as heavy precipitation over Iran has increased with a rise in sinuosity.

4 Conclusions

Given the fast Arctic warming (Holland and Bitz, 2003: 22) and the variation in atmospheric patterns in response to Climate change (Chen et al. 2008), it is of great importance to examine the effects of these changes on climatic elements (Trenberth et al. 1990). The present research investigated the impact of spatial variation in westerlies on widespread and extreme precipitation over Iran. The relationship between 500hPa sinuosity and precipitation upon AO and NAO was examined. The results demonstrate a significant relationship between sinuosity rate and precipitation over the country at the confidence level of 95%. In average, the index of statistical relationship between sinuosity and precipitation over Iran has amounted to 74%. The results of the Mann-Kendall test of trend analysis indicate a decreasing trend in the variation in sinuosity for the 1979-1999 period but an increasing trend for the 2000-2020 period. The overall trend exhibits an increase by 0.0018 per year. The maximum monthly values of sinuosity are observed for January, March, and December, and the minimum is seen for October. The value of sinuosity exhibits decrease in October with respect to the other months and increase in December and March. Overall, the maximum values of atmospheric sinuosity have occurred in 2019, 2011, and 2015, and the minimum has occurred in 2010. The values of sinuosity are accounted for by the sinuous oscillations in atmospheric wave forms given the particular contours, based on which daily precipitation has increased by 3 mm with a rise of 0.2 in the value of sinuosity, monthly precipitation by 10 mm, and the annual value by 38 mm. The relationship between sinuosity and the teleconnection indices has involved the AO index, with a rate of 0.65, and NAO, with 0.52. The positive phases of AO and NAO have been associated with increase in sinuosity and the negative phases with a decrease in most of the years. An increase in the value of atmospheric sinuosity has suggested a rise in wave amplitude and an extension of westerly flows to latitudes lower than 20°N, accompanied by an increase in wave depth, a rise in the atmospheric blocking phenomenon, and the formation of cut off lows. As more cut off lows occur, heavy precipitation increases in monthly and annual scale (Moradi. 2004 and Masoodian 2008). Positive Arctic phases, polar low amplification and consequent trough extension down to Southern Greenland (Hojati and Masoodian 2018) over Atlantic Ocean, and meridian extension of subtropical highs toward higher latitudes result in the prevalence of an intense pressure over the eastern half of Atlantic Ocean and Northern Europe. An intense pressure gradient causes the occurrence of a tilted trough axis and evolution of powerful blocking over Eastern Atlantic, and two powerful cores take shape as the meridian component of high flows is enforced. The initial core is formed over Eastern Atlantic through eastward flows, and the secondary trough core takes shape over the Mediterranean. The role of sinuosity in the middle layers of the atmosphere in widespread and extreme precipitation over Iran indicates the significant impact of spatial variation in westerlies on the changes in surface elements including the widespread precipitation over the region. The increase in the value of sinuosity resulting from the rise in meridian flow enforces the trough and increases precipitation. The temporal diversity in sinuosity is influenced by the increase in the orbital and meridian flow variation. The location of the deep trough center over 20-30°N contributes to the

persistence of precipitation and transfer of moisture from these resources (Alijani et al. 2019). In such conditions, as the polar front and polar jet proceed to middle latitudes over moisture resources, the westerly troughs are drawn in some cases over Red Sea to provide the requirements for cyclogenesis (Alpert et al. 2004). Harman (1991) stated that a high westerly trough at 500hPa is located over the Mediterranean. The results reported in this section are consistent with those of Raziei et al. (2010); Alijani (2002). An important finding of the present study concerns the formation of cut off lows as a result of Eastern Atlantic blocking, as full consistency is observed in all the examined patterns between the cut off low formed in Eastern Mediterranean and the Eastern Atlantic trough. Independent research seems to be needed to investigate how dynamic atmospheric patterns behave upon formation of blocking over the Atlantic and Mediterranean. In general, cut off lows are located in most widespread and extreme precipitation over the country within 35°N 30°W-50°E. An examination of the frequency of cut off lows for the 500hPa 10°N-60°N 0-70°E kernel indicates an increasing trend. An increase in atmospheric sinuosity resulting from the impact of a rise in meridian variation in westerly flows on cut off low values can affect extreme precipitation over Iran under the influence of Climate change (Hamidianpour and khosravi 2020). The increase in sinuosity in March and December, when precipitation exhibits greater intensity (Alijani 1999) can raise flood-like precipitation (Alijani 2011). These conditions can result from variation in synoptic patterns effective on precipitation over the country (Masoodian and Darand 2013), which is far more significant upon climate change.

Declarations

Conflict of Interest The authors declare no competing interests.

Funding Statement Not applicable.

Author's Contribution Conceptualization; Formal analysis; Investigation;

Methodology; Resources; Software; Validation; Visualization; Writing, review and editing: Nabi mirzaei, Mohammad Darand, Bohloul Alijani, Zahra hejazizaded, Mohammad hossein nasserzadeh. Writing, original draft. Preparation: Mohammad Darand and Nabi mirzaei.

Availability of data and material The ECMWF data is at https://www.ecmwf.int/en/forecasts/datasets, Precipitation data at https://data.irimo.ir/. Material Does not exist.

Code availability Not applicable.

Ethics approval Not applicable.

Consent to participate Not applicable.

Consent for publication Not applicable.

References

1. Abatzoglou JT, Williams AP (2016) Impact of anthropogenic climate change on wildfire across western US forests. Proc Natl Acad Sci U S A 113(42):11770–11775. https://doi.org/10.1073/pnas.1607171113
2. Alijani B (1999) Oscillation Temporal and spatial geopotential height of 500 hPa in the Mediterranean and its effect on the climate of Iran in February. Proceeding of the second regional conference of climate change
3. Alijani B (2011) spatial analysis of critical temperatures and daily precipitation in Iran. J Geogr Sci 20:9–30
4. Aljani B (2002) Variation of 500 hPa flow patterns over Iran and surrounding areas and their relationship with the climate of Iran. Theor Appl Climatol 71:41–44. 10.22108/gep.2017.97959.0
5. Alijani B, Nezamati H (2017) Spatial and Temporal Analysis of the Mediterranean Trough. J Geogr Environ Plan 28(2):79–92. https://www.sid.ir/en/journal/ViewPaper.aspx?id=566802
6. Alijani B (2019) Quantitative methods in geography. Samat, Tehran
7. Alijani B, Mirzaei N, Jahedi A (2020) A Synoptic analysis comprehensive and heavy rainfall in Iran: case study16-31 st 2019. Journal Climate Change Hazards 1(2):70–114
8. Alpert P, Osetinsky I, Ziv B, Shafir H (2004) Semi-objective classification for daily synoptic systems: Application to the eastern Mediterranean climate change. Int J Climateatol 24(8):1001–1011
9. Allen MR, Ingram WJ (2002) Constraints on future changes in climate and the hydrologic cycle. Nature 419(6903):228–232
10. Azizi GH, Moradi M, Rezaei (2018) Identification and Climatology of Cut-off Lows over Iran and relationship with NAO, ENSO. J Geogr Res 128(5):15–27
11. Babaifini A, Farajzadeh M (2002) Patterns of spatial and temporal rainfall changes in Iran. Human Sciences modares 6(27):51–70
12. Bacon S, Carter DJT (1991) Wave climate changes in the North Atlantic and North Sea. Int J Climatol 11(5):545–558. https://doi.org/10.1002/joc.3370110507
13. Bannayan M, Lotfabadi SS, Sanjani S, Mohamadian A, Aghaalikhani M (2011) Effects of precipitation and temperature on crop production variability in northeast Iran. Int J Biometeorol 55(3):387–401
14. Barnes EA, Polvani L (2013) Response of the multitude jets, and of their variability, to increased greenhouse gases in the CMIP5 models. Int J Climateatol 26(18):7117–7135
15. Barnes EA (2013) Revisiting the evidence linking Arctic amplification to extreme weather in midlatitudes. Geophys res Lett 40(17):4734–4739
16. Bogardi I, Matyasovszky I, Bardossy A, Duckstein L (1994) A Hydroclimatological Model of Areal Drought. J Hydrol 153(1):245–264
17. Boucher JP, Bakheit MA, Nechtschein M, Villa M, Bonera G, Borsa F (1976) High-temperature spin dynamics in the one-dimensional Heisenberg system (C H 3) 4 NMn Cl 3 (TMMC): Spin diffusion, intra-and interchain cut off effects. Phys Rev B 13(9):40–98

18. Castillo CGM (2020) A midlatitude climatology of 200-and 500-hPa cut-off lows and its usefulness in categorizing cut-off lows in central Chile. The University of Manchester
19. Cattiaux J, Peings Y, Saint- Martin in D Trou-Kechout N Vavrus SJ (2016) Sinuosity of midlatitude atmospheric flow in a warming world. Geophys res Lett 43(15):8259–8268. https://doi.org/10.1002/2016GL070309
20. Chen G, Lu J, Frierson DM (2008) Phase speed spectra and the latitude of surface westerlies: Internal variability and global warming trend. Int J Climateatol 21(22):5942–5959. https://doi.org/10.1175/2008JCLI2306.1
21. Darand M, Mirzaei N (2019) The relationships between precipitation amounts, number of rain days, and relative vorticity in the mid-troposphere over Iran. Weather 74:23–31. https://doi.org/10.1002/wea.3391
22. Davenport FV, Burke M, Deffenbaugh NS (2021) Contribution of historical precipitation change to US flood damages. Proc Natl Acad Sci 118 (4). https://doi.org/10.1073/pnas.2017524118
23. Delhasse A, Kittel C, Amory C, Hofer S, As DVS, Fausto R, Fettweis X (2020) Brief communication: Evaluation of the near-surface climate in ERA5 over the Greenland Ice Sheet. The Cryosphere 14(3):957–965
24. Di Napoli C, Barnard C, Prudhomme C, Cloke HL, Pappenberger F (2021) ERA5-HEAT: A global gridded historical dataset of human thermal comfort indices from climate reanalysis. Geosci Data J 8(1):2–10
25. Ding F, Li C (2017) Subtropical westerly jet waveguide and winter persistent heavy rainfall in south China. J Geophys Res Atoms 122(14):7385–7400
26. Dorn W, Dethloff K, Rinke A, Roeckner E (2003) Competition of NAO regime changes and increasing greenhouse gases and aerosols with respect to Arctic climate projections. Clim Dyn 21(5):447–458
27. Dullaart JC, Muis S, Bloemendaal N, Aerts JC (2020) Advancing global storm surge modelling using the new ERA5 climate reanalysis. Clim Dyn 54(1):1007–1021
28. Faris R, Moody J (1999) Blocking the Future. Soc Sci Hist 23:501–533. https://doi.org/10.1017/S0145553200021854
29. Gong DY, Gao Y, Guo D, Mao R, Yang J, Hu M, Gao M (2014) Interannual linkage between Arctic/North Atlantic Oscillation and tropical Indian Ocean precipitation during boreal winter. Clim dyn 42(3-4):1007–1027
30. Hamidainpour M, khosrowi M (2020) The Impact of global warming in the spring rains of spring 1398 in western Iran, Sixth Regional Conference Climate Change, Iran
31. Harman JR (1991) Synoptic climatology of the westerlies. Process and patterns
32. Hitchman MH, Rowe SM (2021) On the Formation of Tropopause Folds and Constituent Gradient Enhancement near Westerly Jets. J Atmos Sci 78(7):2057–2074. https://doi.org/10.1175/JAS-D-20-0013.1

33. Holland MM, Bitz CM (2003) Polar amplification of climate change in coupled models. Clim Dyn. 21(3-4): 221-232. https://link.springer.com/article/10.1007%2Fs00382-003-0332-6
34. Hojati Z, Masoodian SA (2021) Mid Latitude Atmospheric Circulation and its Relation with Temperature Variations in Iran. Geogr Dev 19(62):31–52
35. Hojati Z, Masoodian SA (2018) Relationship between Arctic Oscillation and Precipitation in Iran. Phys Geogr Res Q 50(3):577–591. Doi 10.22059/jphgr.2018.244741.1007135
36. Hombari FJ, Barati G, Moradi M (2020) Evaluation of the Relationship between Blocking Patterns and Duration of Spring Frost Waves: The Case of Iran. J Meteorol Res 34(3):586–600
37. Huang H, Cui H, Ge Q (2021) Assessment of potential risks induced by increasing extreme precipitation under climate change. Nat Hazards 5(3):1–21
38. Hu Q, Feng S (2010) Influence of the Arctic oscillation on central United States summer rainfall. J Geophys Res Atoms 115:D1
39. Krishnamurti TN, Tewari M, Rajendran K, Gadgil S (2002) A heavy winter monsoon rainfall episode influenced by easterly waves, a westerly trough, blocking and the ITCZ. Weather 57(10):367–370
40. Lauterbach S, Witt R, Plessen B, Dulski P, Prasad S, Mingram J, Schwalb A (2014) Climatic imprint of the mid-latitude Westerlies in the Central Tian Shan of Kyrgyzstan and teleconnections to North Atlantic climate variability during the last 6000 years. The Holocene 24(8):970–984
41. Liu J, Curry JA, Wang H, Song M, Horton RM (2012) Impact of declining Arctic sea ice on winter snowfall. Proc Nation Acad Sci 109(11):4074–4079
42. Lupo AR, Clark JV, Hendin AM, Kelly AS, Mihalka KM, Perrin BL, Puricelli KM (2008) The Global Increase in Blocking Occurrences, In Proceedings of the 20th Conference on Global Climate Change American. Meteorol Soc 19 – 24 January
43. Martin JE, Vavrus SJ, Wang F, Francis JA (2016) Sinuosity as a measure of middle tropospheric waviness 6. J Clim 25(26)
44. Masoodian SA (2008) Relationship between North Atlantic Oscillation and Precipitation in Iran. J Geogr Res 23(4):3–18
45. Masoodian SA, Darand M (2013) Recognition and Analysis of Variation in Extreme Precipitation Indices during Recent Decades. Geogr Reg Dev11 (20)
46. Moradi HR (2004) North Atlantic Oscillation index and its effect on climate in Iran. Geographical Research Quarterly 48(5):17–30
47. Munoz C, Schultz DM (2021) Cut off Lows, Moisture Plumes, and Their Influence on Extreme-Precipitation Days in Central Chile. J Appl Meteorol Clim 60(4):437–454
48. Miyakoda K, Gordon T, Caverly R, Stern W, Sirutis J, Bourke W (1983) Simulation of a blocking event in January 1977. Mon Weather Rev 111(4):846–869
49. Pavlovic Berdon N (2012) The impact of Arctic and North Atlantic Oscillation on temperature and precipitation anomalies in Serbia. Geogr Pannon 16(2):44–55

50. Raziei T, Mofidi A, Zarrin A (2009) Centers of activity and patterns of large-scale atmospheric circulation of 500 hPa on the Middle East and their relationship with rainfall in Iran. Journal of the Earth Space Physics 35(1):121–141
51. Schinke H (1993) On the occurrence of deep cyclones over Europe and the North Atlantic in the period 1930-1991. Contributions to atmospheric physics 66(3):223–237
52. Sen Roy S (2009) A spatial analysis of extreme hourly precipitation patterns in India. Int J Climatol 29:345–355
53. Singleton AT, Reason CJC (2007) Variability in the characteristics of cut-off low pressure systems over subtropical southern Africa. Int J Climatol 27(3):295–310
54. Singh D, Tsiang M, Rajaratnam B, Diffenbaugh NS (2013) Precipitation extremes over the continental United States in a transient, high-resolution, ensemble climate model experiment. J Geophys Res: Atoms 118(13):7063–7086
55. Stein O, Hense A (1994) A reconstructed time series of the number of extreme low pressure events since 1880. Meteorol Z 3(1):43–46
56. Swain DL, Wing OE, Bates PD, Done JM, Johnson KA, Cameron DR (2020) Increased flood exposure due to climate change and population growth in the United States. Earths Future 8(11). https://doi.org/10.1029/2020EF001778
57. Tabari H (2021) Extreme value analysis dilemma for climate change impact assessment on global flood and extreme precipitation. J Hydrol 593, 125932. https://doi.org/10.1016/j jhydrol
58. Trenberth KE, Large WG, Olson JG (1990) The mean annual cycle in global ocean wind stress. J Phys Ocean 20(11):1742–1760
59. Tyrlis E, Tymvios FS, Giannakopoulos C, Lelieveld J (2015) The role of blocking in the summer 2014 collapse of Etesians over the eastern Mediterranean. J Geophys Res: Atoms 120(14):6777–6792. https://doi.org/10.1002/2015JD023543
60. Vavrus SJ, Wang F, Martin JE, Francis JA, Peings Y, Cattiaux J (2017) Changes in North American atmospheric circulation and extreme weather: Influence of Arctic amplification and Northern Hemisphere snow cover. J Clim 30(11):4317–4333. .https://doi.org/10.1175/JCLI-D-16-0762.1
61. Van Loon H, Williams J (1976) The connection between trends of mean temperature and circulation at the surface: Part I. winter. Month Weather Rev 104(4): 365–380. https://doi.org/10.1175/1520-0493(1976)104<0365:TCBTOM>2.0.CO;2
62. Vicente-Serrano SM, López-Moreno JI (2006) The influence of atmospheric circulation at different spatial scales on winter drought variability through a semi-arid climatic gradient in Northeast Spain. International Journal of Climatology J Roy Meteorol Soc 26(11):1427–1453. https://doi.org/10.1002/joc.1387
63. Yadav RK, Rupa Kumar K, Rajeevan M (2009) Increasing influence of ENSO and decreasing influence of AO/NAO in the recent decades over northwest India winter precipitation. J Geophys Res Atmos 114(D12). https://doi.org/10.1029/2008JD011318

64. Zolfagari H, Masoum Pour J, Naser khani A, Miri M (2011) The Effect of blocking systems on the occurrence and continuation of dry and wet periods in the north-west portion of Iran. Geogr Stud dry Reg 3(9):101–119

Figures

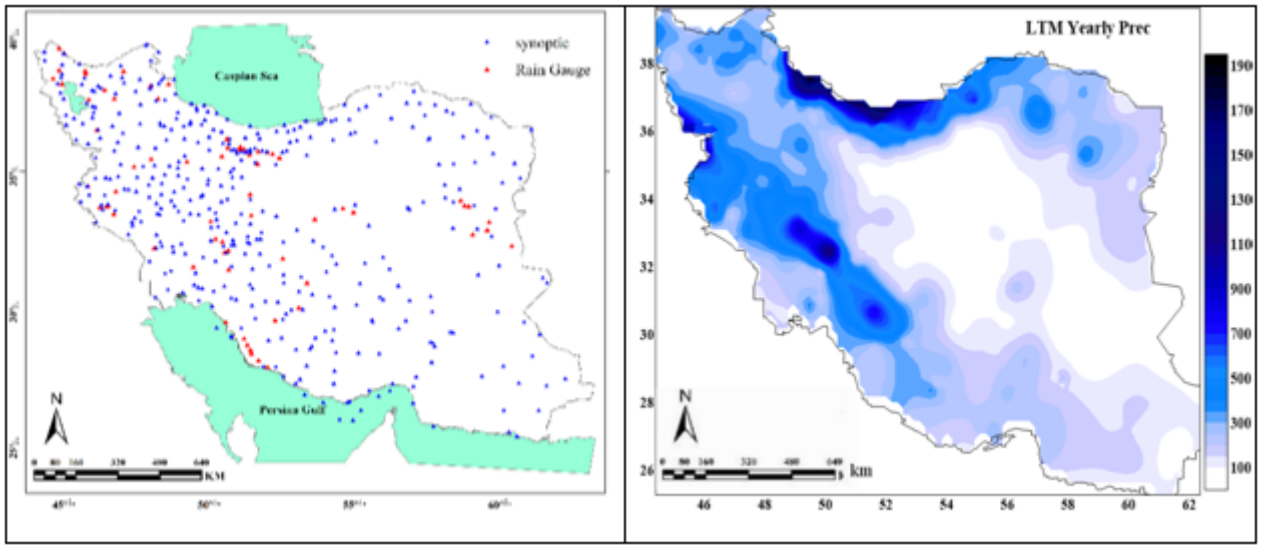

Figure 1

Spatial distribution of Synoptic and gauge Stations, long Term Precipitation (mm) for the period from1979 to 2020

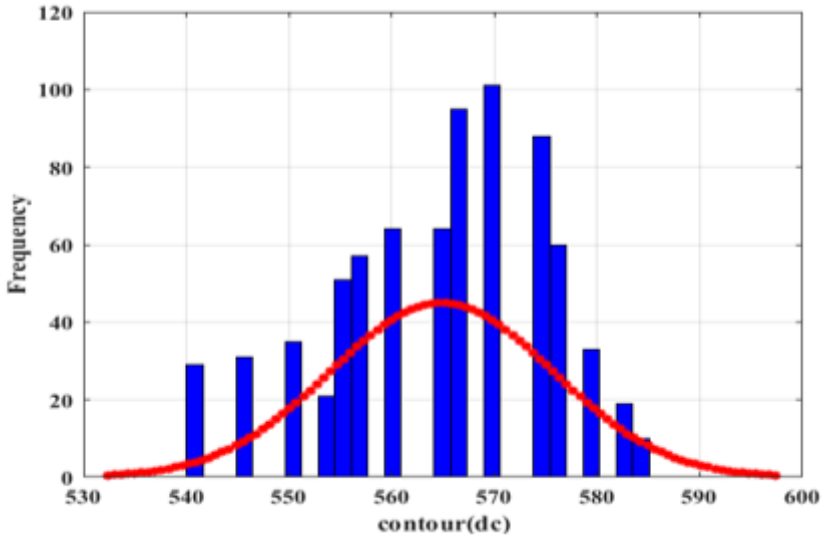

Figure 2

Frequency of contour (decameter) of the Geopotential height inside the borders of Iran during comprehensive and heavy rainfall Event (significant at the 95% confidence level)

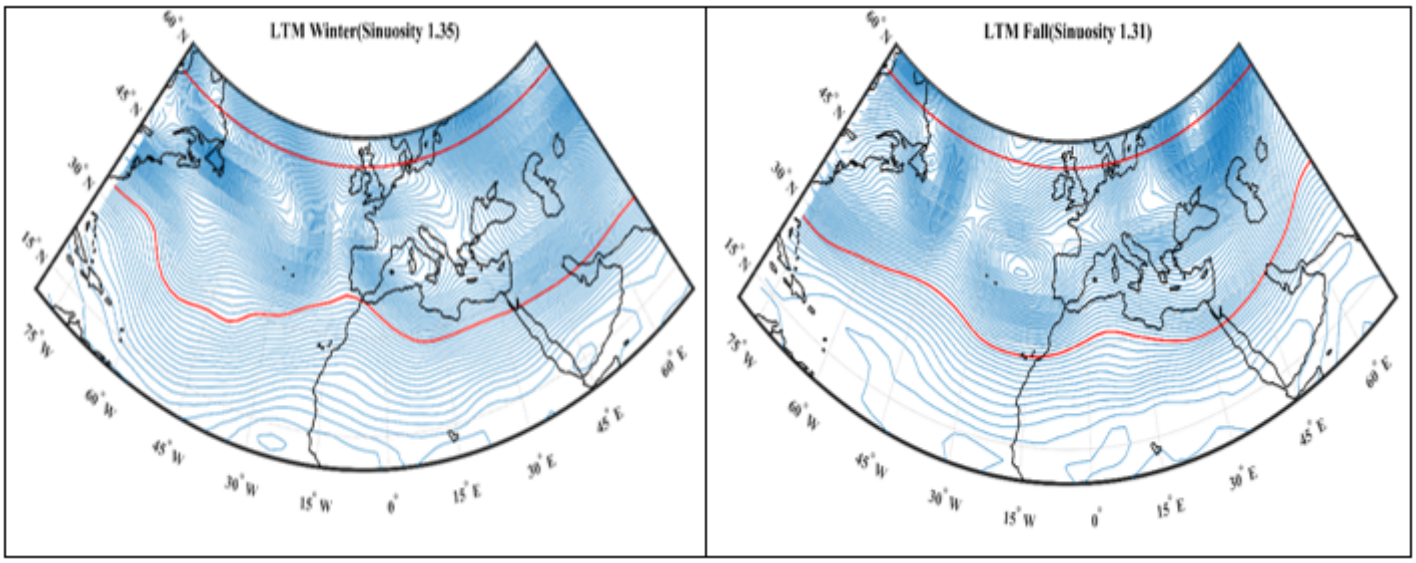

Figure 3

Long-term mean sinuosity of winter and fall from 1979 to 2020

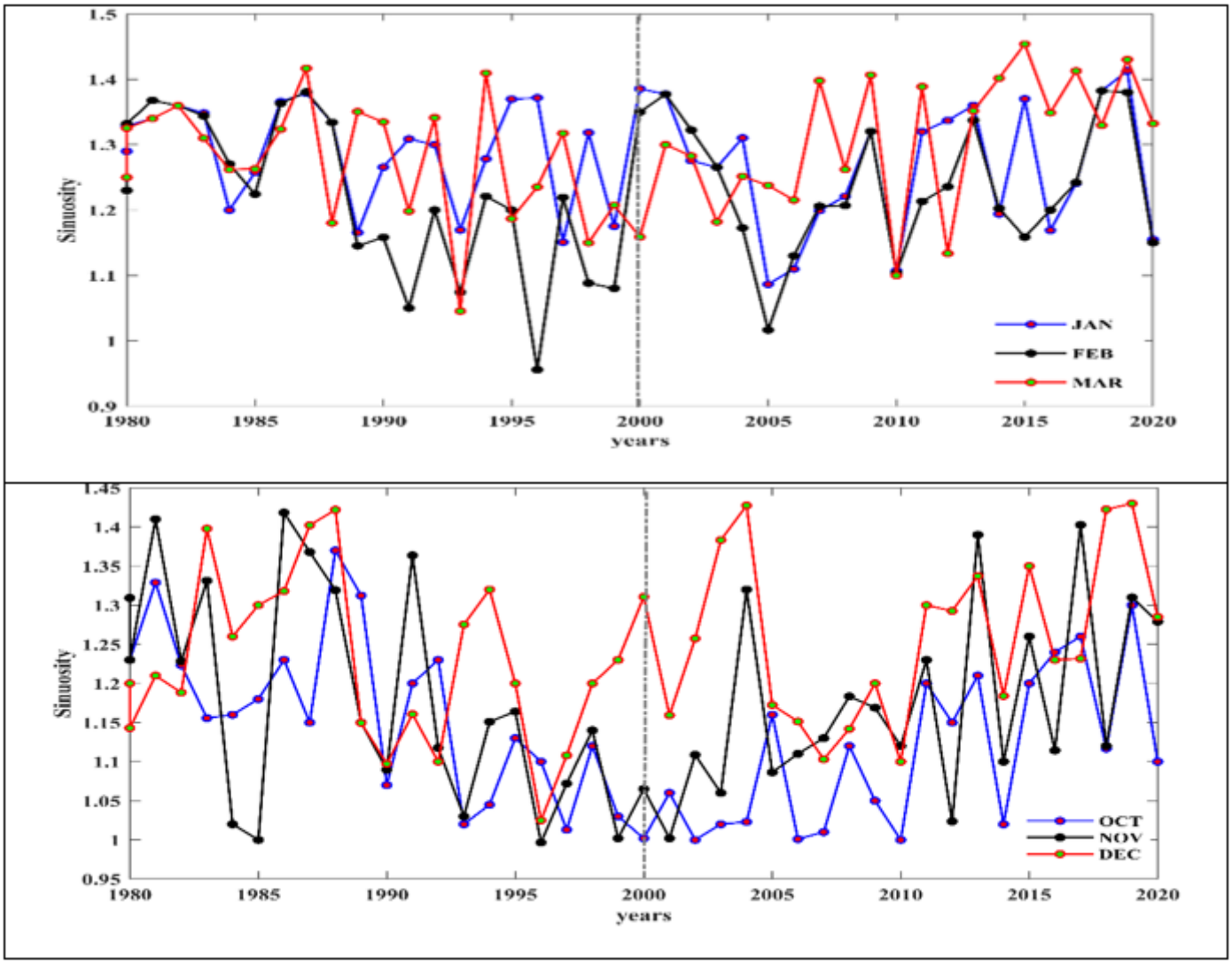

Figure 4

Long-term mean monthly sinuosity -80W to 70E, 10 to 60N

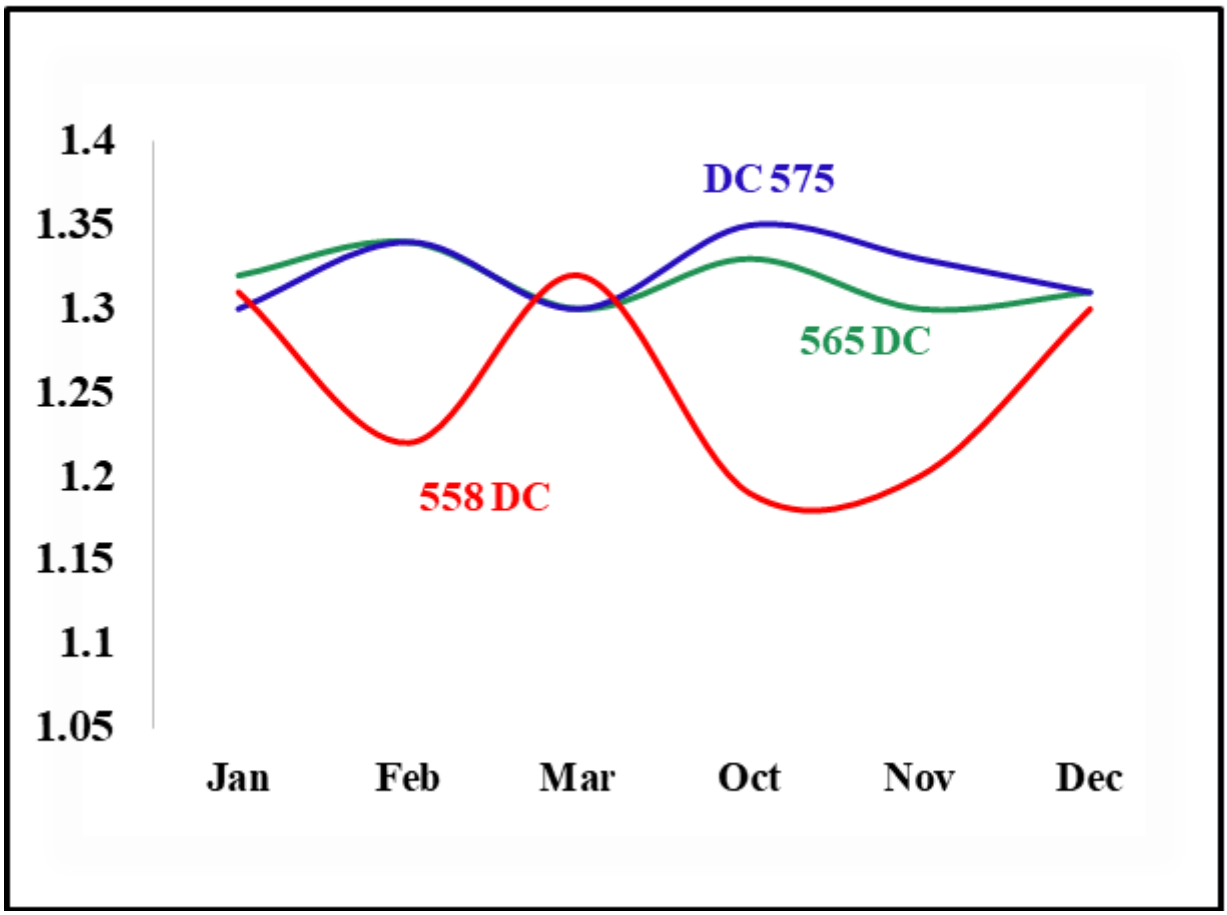

Figure 5

Long-term mean monthly sinuosity for contour 575, 565 and 558 decameter over the area -80W to70E, 10 to 60N

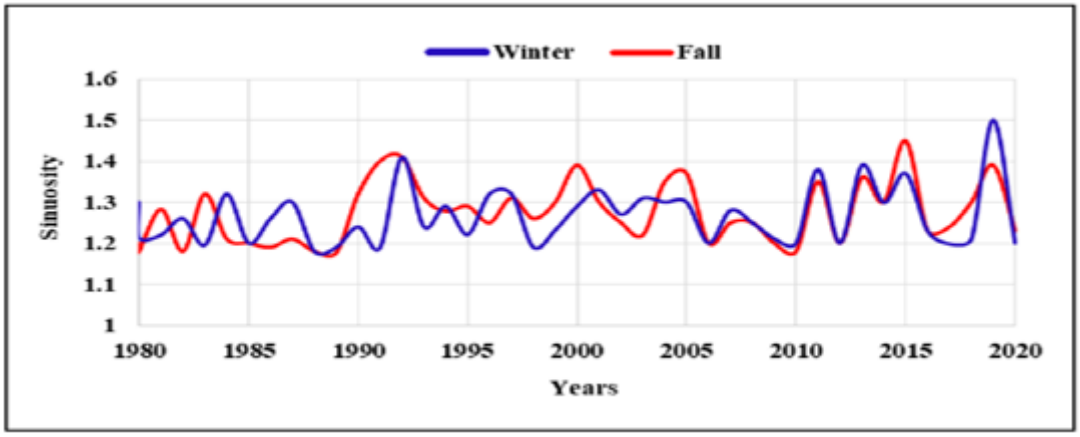

Figure 6

Average Seasonal sinuosity over the area -80E to70W, 10 to 60N during the period from 1979 to 1920

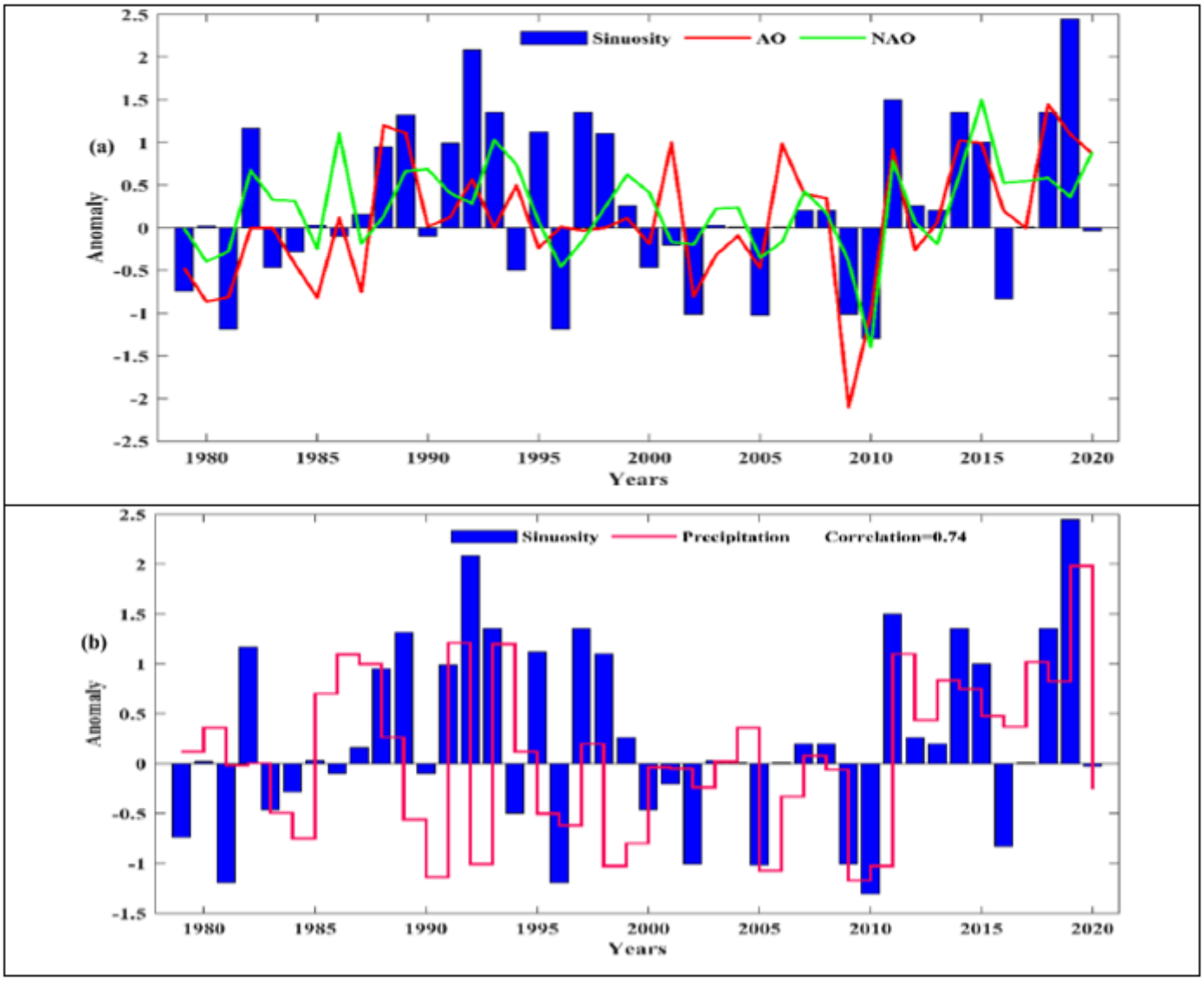

Figure 7

sinuosity anomalies, NAO, AO Oscillation (a), sinuosity anomalies and precipitation over the area -80W to 70E, 10 to 60N(b)

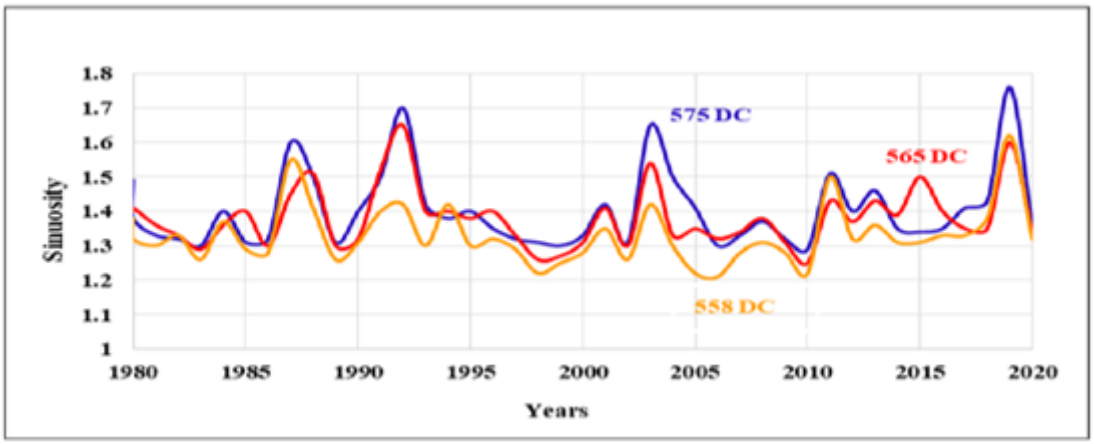

Figure 8

Sinuosity 500 hPa level Contour during comprehensive and heavy rainfall over the area 0 to70E, 10 to 60N

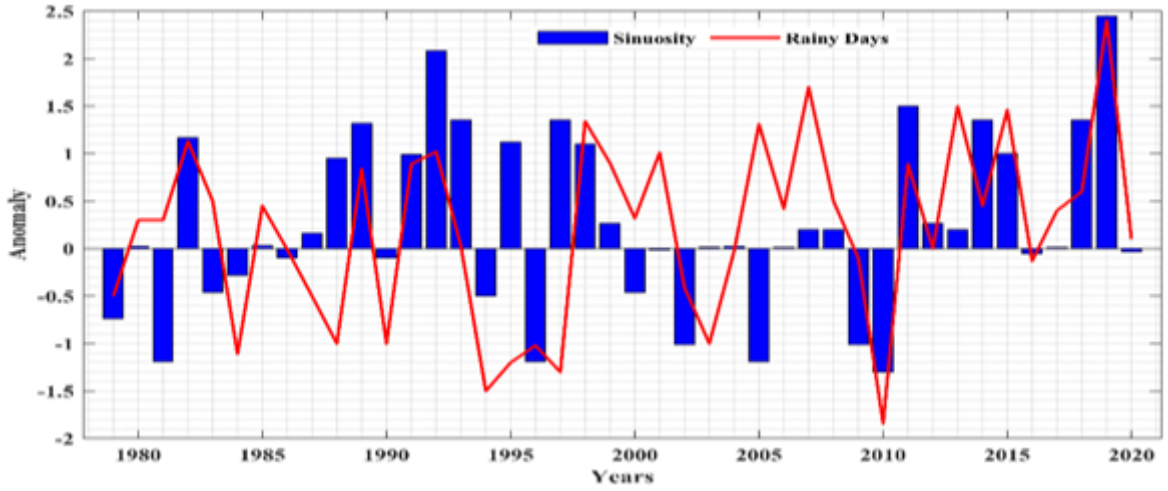

Figure 9

The relationships between sinuosity values at 500 hPa level and frequency of rainy days for over the area 0 to70W, 10 to 60N

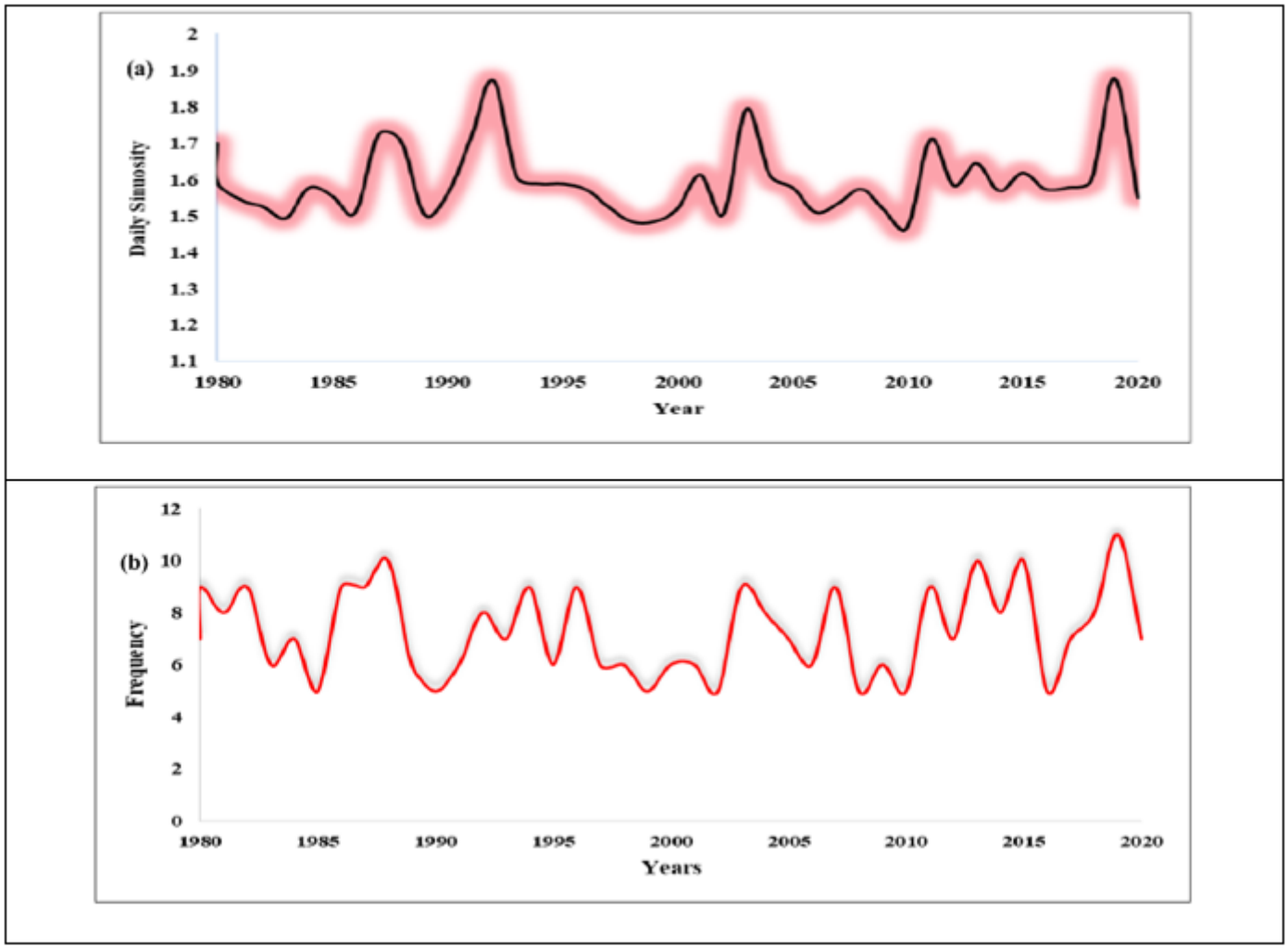

Figure 10

Aggregate sinuosity (a) and frequency of rainy days with heavy rainfall (95% percentile) over the area 0 to70W, 10 to 60N (b)

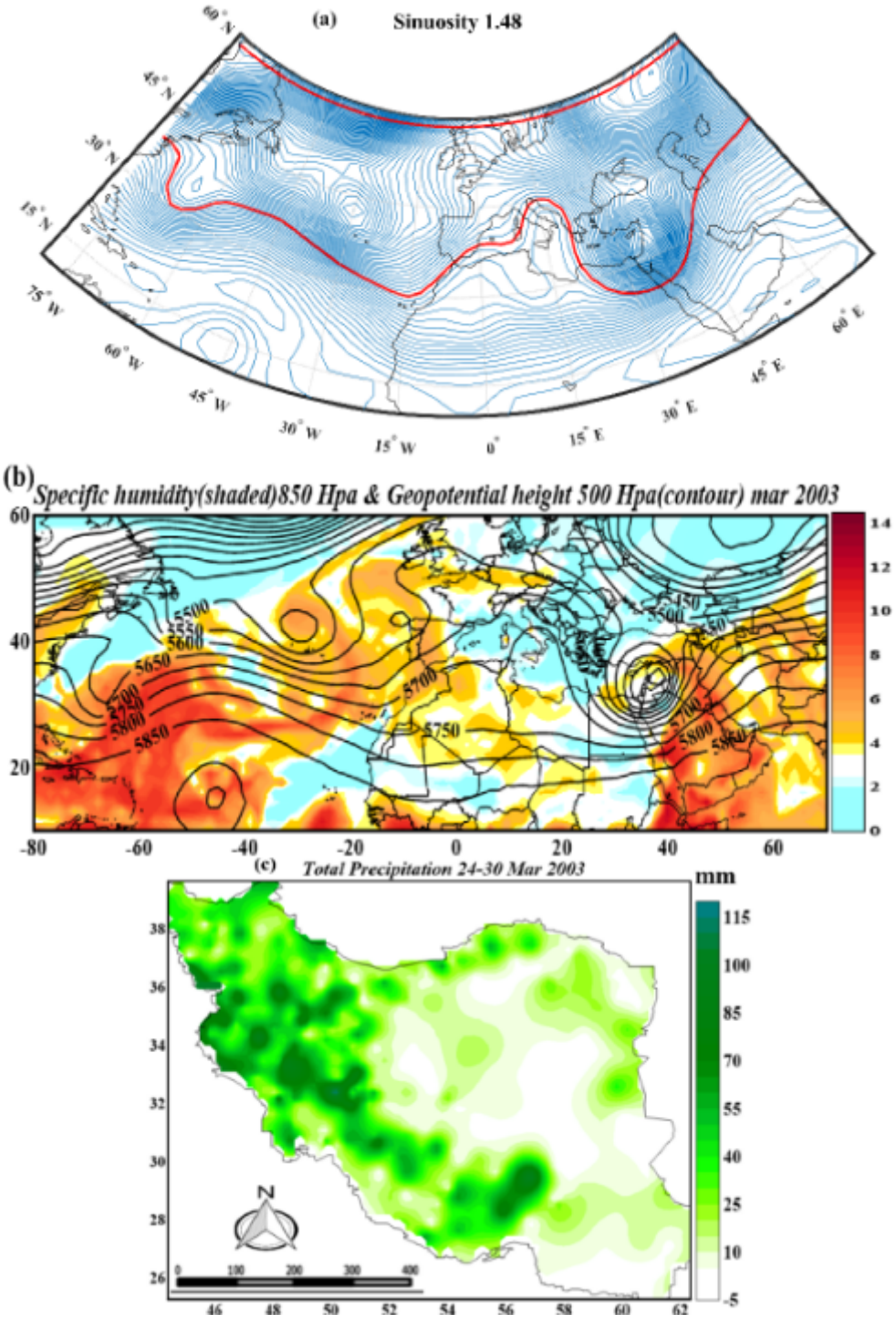

Figure 11

Sinuosity (a), geopotential height at the 500 hPa level and specific humidity at 850hPa (b) and Total precipitation 24 to 30 Mar 2003(c)

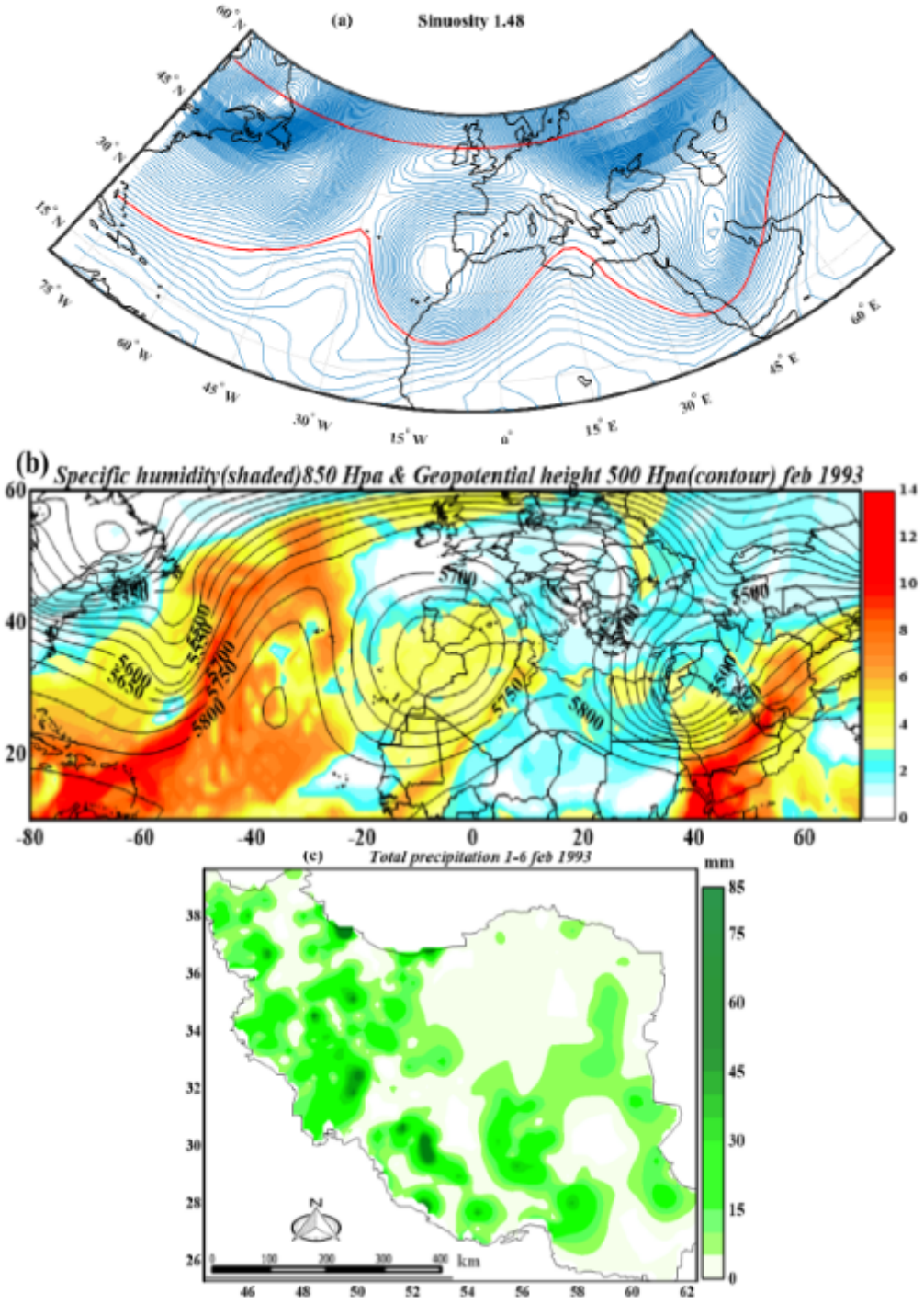

Figure 12

Sinuosity (a), geopotential height at the 500hPa level and specific humidity at 850hPa (b) and Total precipitation 1 to 6 Feb 1993(c)

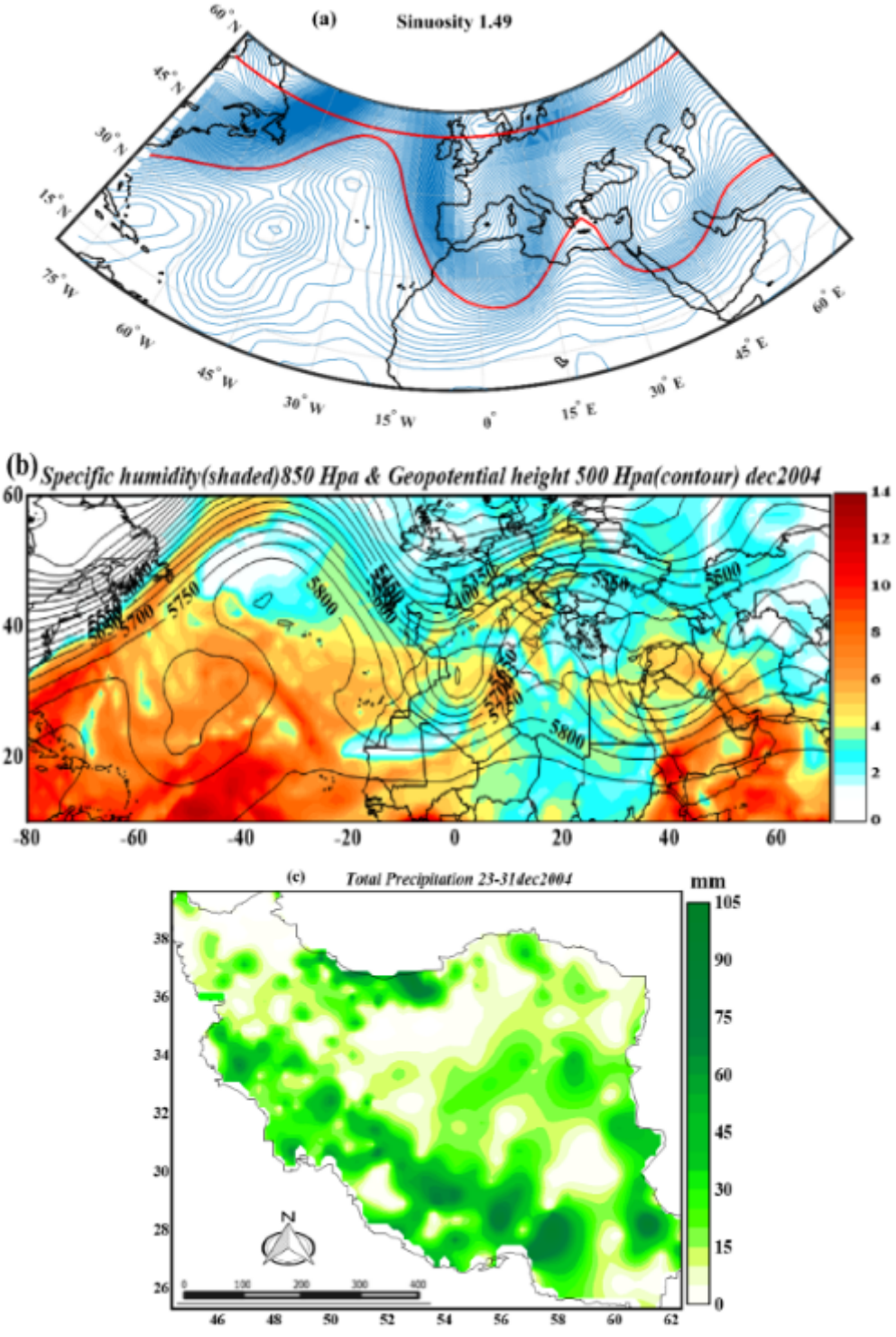

Figure 13

Sinuosity (a), geopotential height at the 500 hPa level and specific humidity at 850hPa (b) and Total precipitation 23 to 31 Dec 2004(c)

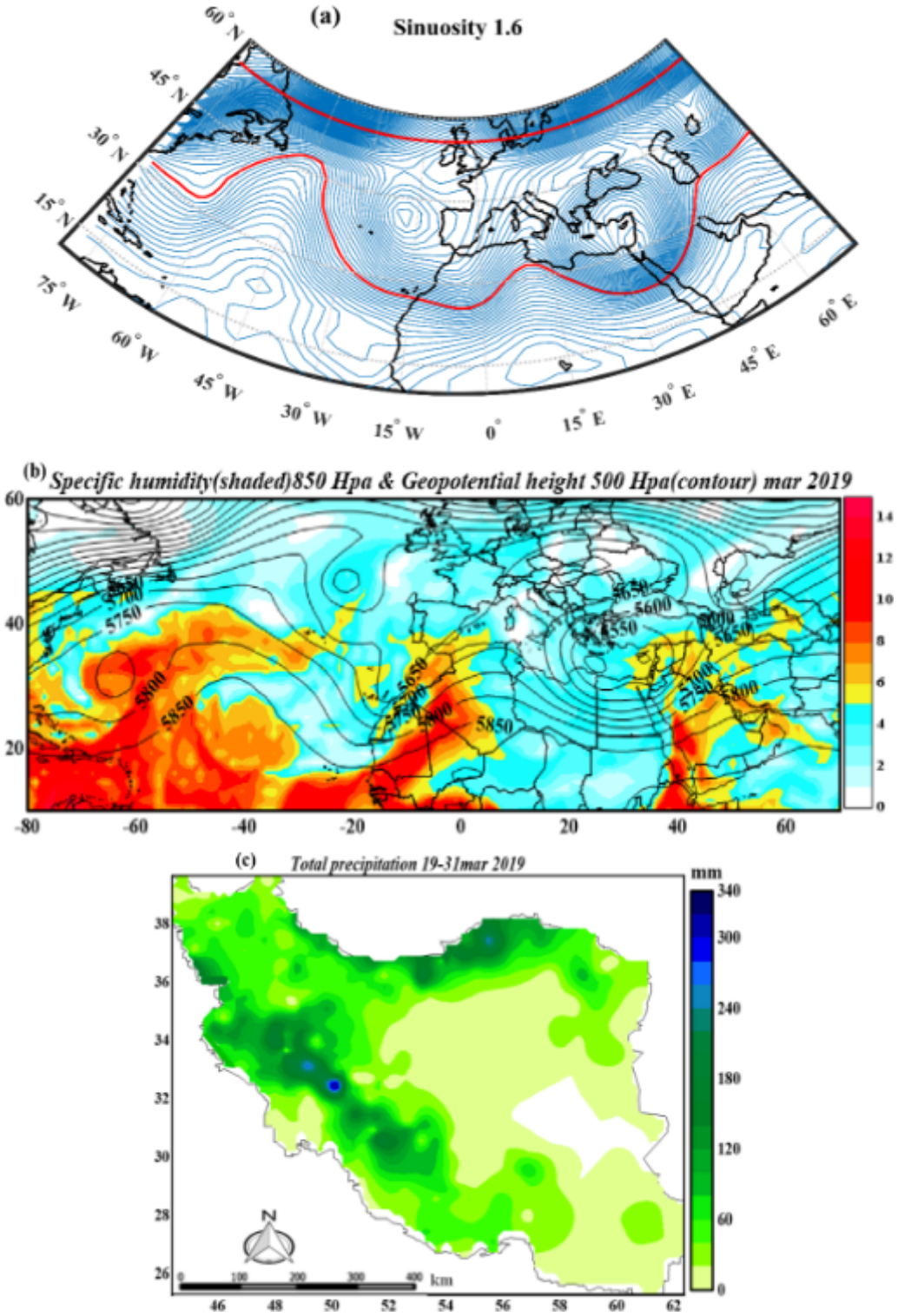

Figure 14

Sinuosity (a), geopotential height at the 500 hPa level and specific humidity at 850hPa (b), and Total precipitation 19-31 Mar 2019 (c)

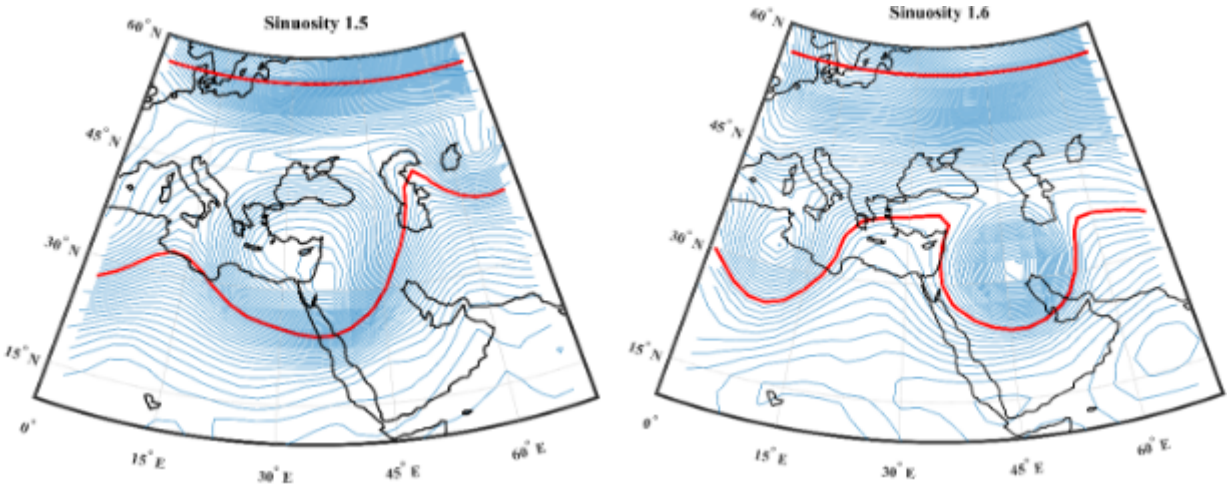

Figure 15

Cases cut of low during comprehensive and heavy rainfall over the area 0 to70W, 10 to 60N

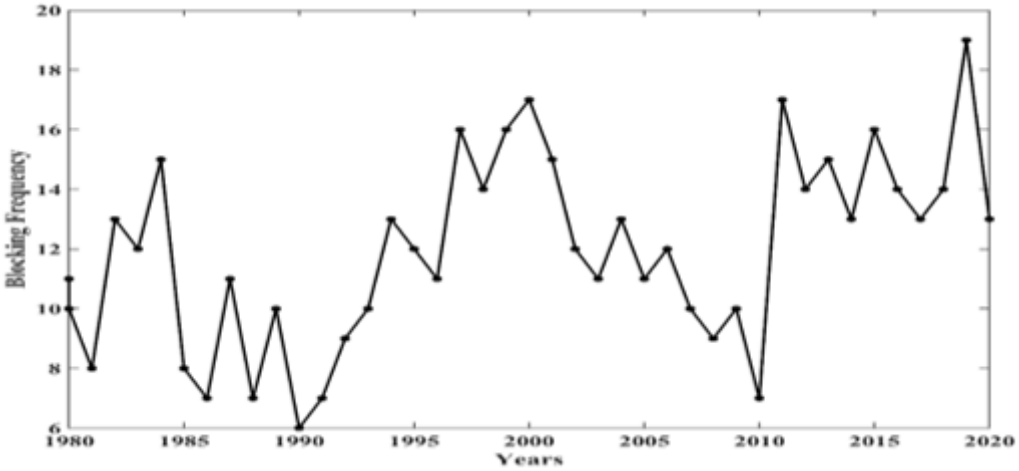

Figure 16

Annual frequency of blocking at the 500 hPa level over the area 0 to70W, 10 to 60N from 1979 to 2020

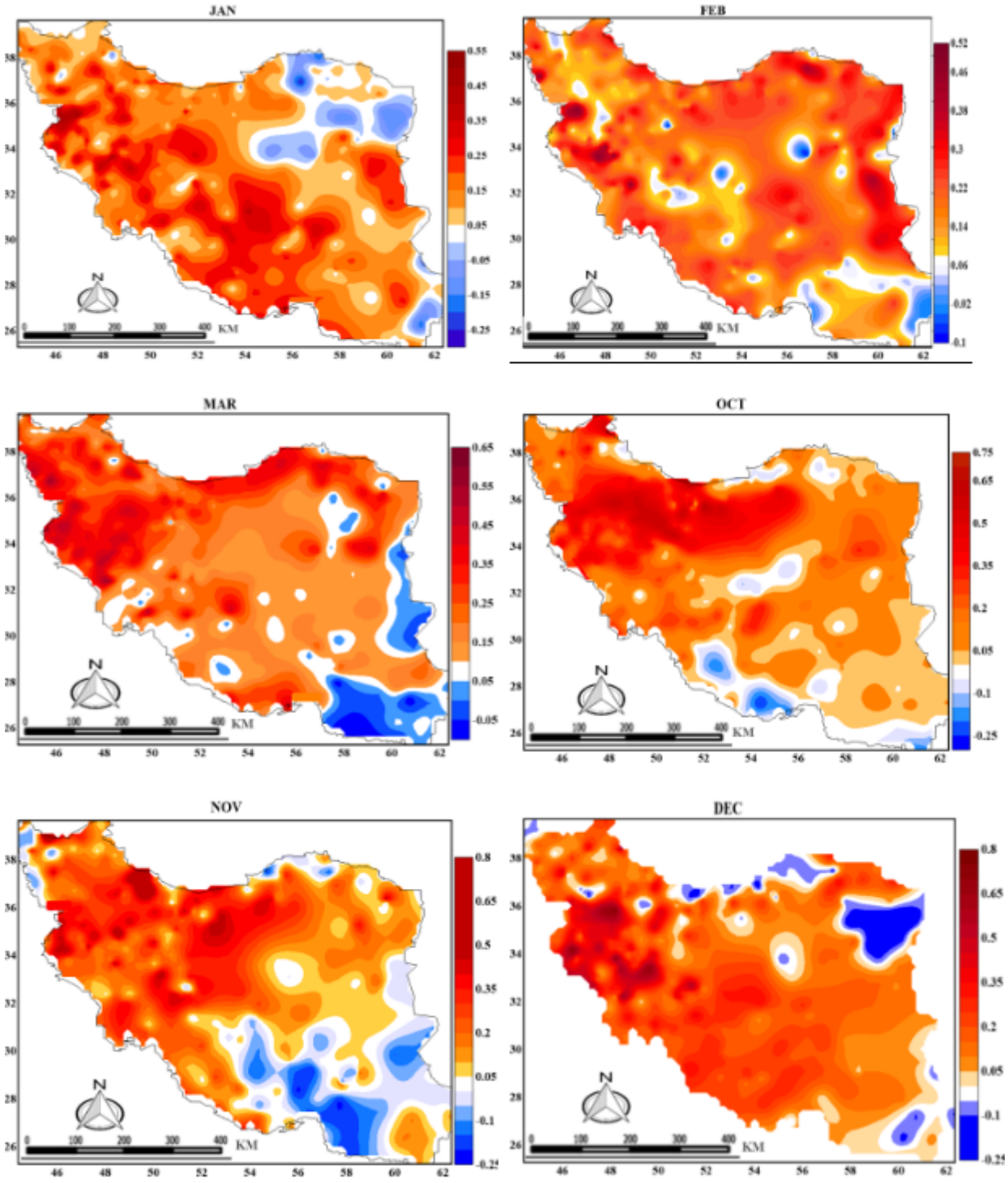

Figure 17

The correlation between monthly precipitation and sinuosity at the 500 hPa level (significant at the 95% confidence level) from 1979 to 2020